Supplementary Informations for

Spin-Selective Orbital Reconfiguration and Colossal Nonlinear Anisotropy in Defect-Engineered Atomically Thin Quantum Dots

Saraf Mohaimen Chowdhury[a], Salena Akther[b,c]

[a]Department of Electrical and Electronic Engineering, Port City International University, Chattogram 4202, Bangladesh

[b]Department of Natural Science, Port City International University, Chattogram 4202, Bangladesh
[c]Department of Mathematics, Chittagong University of Engineering and Technology, Chattogram 4349, Bangladesh

Contents

1 Computational Methods

The DFT calculation was performed using the hybrid exchange energy of the ωB97X-D functional [1], which is expressed as:

$$E_{\mathrm{X}}^{\omega\mathrm{B97X}} = a_{\mathrm{SR}} E_{\mathrm{X}}^{\mathrm{HF,SR}} + (1 - a_{\mathrm{SR}}) E_{\mathrm{X}}^{\mathrm{DFT,SR}} + E_{\mathrm{X}}^{\mathrm{HF,LR}}$$

Where:

- $a_{\mathrm{SR}} = 0.22$ is the fraction of short-range exact (Hartree–Fock) exchange,
- $E_{\mathrm{X}}^{\mathrm{HF,SR}}$ is the short-range Hartree–Fock exchange energy,
- $E_{\mathrm{X}}^{\mathrm{DFT,SR}}$ is the short-range DFT exchange energy,
- $E_{\mathrm{X}}^{\mathrm{HF,LR}}$ is the long-range Hartree–Fock exchange energy.

where the range-separation parameter is:

$$\omega = 0.2\,\mathrm{bohr}^{-1}$$

The LANL2DZ basis set was used, which combines a double-ζ valence basis with the Los Alamos effective core potential (ECP) [2], to replace inner-core electrons with a simplified potential. The orbital energy gap was derived from the difference between the highest occupied and lowest unoccupied frontier orbitals, and systems with a closed-shell minimum corresponds to $E_g(\alpha) = E_g(\beta)$. The binding energies of all structures were calculated using the following equations to quantify the strength of atomic interactions:

$$\mathrm{E}_b = \frac{n_{\mathrm{m}}\mathrm{E}_{\mathrm{m}} + n_{\mathrm{c}}\mathrm{E}_{\mathrm{c}} + n_{\mathrm{d}}\mathrm{E}_{\mathrm{d}} - \mathrm{E}_{\mathrm{t}}}{n_{\mathrm{t}}} \tag{1}$$

where n_{m}, n_{c}, n_{d}, and n_{t} are the number of metal atoms, chalcogen atoms, dopant atoms, and the total number of atoms, respectively. E_{m}, E_{c}, E_{d}, and E_{t} are the corresponding energies.

The directional components of the g-tensor were calculated using the GIAO formalism [3], where the rotational **g**–tensor derived from the second-order response of the ground-state energy (E) with respect to perturbations by an external magnetic field ($\vec{\mathbf{B}}$) applied along the Cartesian axes. Conceptually, this can be expressed as the linear response of the angular momentum expectation value to the applied magnetic field, i.e.,

$$g_{\lambda\eta} \propto \frac{d}{dB_\lambda} \left\langle \Psi(B) \middle| \hat{J}_\eta \middle| \Psi(B) \right\rangle \Big|_{B=0}$$

where $\Psi(B)$ is the field-perturbed ground-state wavefunction, and $\hat{J}_\eta$ is the angular momentum operator. The deviation from the free-electron reference was then obtained for each principal direction as:

$$\Delta g_{ii} = g_{ii} - g_e \tag{2}$$

The static nonlinear components were calculated and reported using the finite-field method [4] within the same theoretical framework. The system's energy under an external electric field $\mathbf{E}$ can be expanded as:

$$E = E^0 - \mu_i E_i - \frac{1}{2}\alpha_{ij}E_iE_j - \frac{1}{6}\beta_{ijk}E_iE_jE_k - \frac{1}{24}\gamma_{ijkl}E_iE_jE_kE_l + \cdots,$$

where μ_i, α_{ij}, β_{ijk}, and γ_{ijkl} denote the dipole moment, polarizability, first-order hyperpolarizability, and second-order hyperpolarizability tensors, respectively. The isotropic polarizability was defined as the scalar average

$$\alpha_0 = \frac{1}{3}\mathrm{Tr}(\alpha_{ij}), \tag{3}$$

and the anisotropic polarizability $\Delta\alpha$ is evaluated as,

$$\Delta\alpha = \sqrt{\frac{1}{2}\left[(\alpha_{xx}-\alpha_{yy})^2 + (\alpha_{yy}-\alpha_{zz})^2 + (\alpha_{zz}-\alpha_{xx})^2 + 6(\alpha_{xy}^2+\alpha_{yz}^2+\alpha_{xz}^2)\right]} \tag{4}$$

and to capture the anisotropic response of the first- and second-order hyperpolarizabilities specific to the planar geometry of 2D nanoflakes, the hyperpolarizability tensors were decomposed into *in-plane* (parallel, x- and y-directions) and *out-of-plane* (perpendicular, z-direction) components:

$$\beta_{\parallel} = \frac{1}{2}(\beta_{xxx} + \beta_{yyy}), \quad \beta_{\perp} = \beta_{zzz}, \tag{5}$$

$$\gamma_{\parallel} = \frac{1}{2}(\gamma_{xxxx} + \gamma_{yyyy}), \quad \gamma_{\perp} = \gamma_{zzzz}. \tag{6}$$

Projected density of states (PDOS) for s, p, and d orbitals, as well as for individual atomic groups, was calculated using molecular orbital energies and coefficients. A Gaussian broadening of $\sigma = 0.28$ eV was applied on a uniform energy grid of 4000 points. Both total and resolved contributions are plotted. States below a 1×10^{-6} a.u. threshold were excluded to avoid numerical noise. Molecular orbital isosurfaces were visualized at ± 0.02 a.u., and the isovalues for spin density and electron density contours were set to 0.0004 a.u. Post-processing of the orbital wavefunctions was carried out using the ***Multiwfn*** program, and all real-space numerical integrations were performed using *Python*.

2 Structural Parameters

GaS Nanoflake
Maximum diameter ($D_{\max}$): 12.733 Å
Corrugation: 0.000 Å
Radius of gyration (R_g): 5.021 Å
Average bond length: 2.345 Å
Smallest bond length: 2.130 Å
Largest bond length: 2.625 Å

GaS:Zr Nanoflake
Maximum diameter ($D_{\max}$): 13.110 Å
Corrugation: 0.000 Å
Radius of gyration (R_g): 5.034 Å
Average bond length: 2.366 Å
Smallest bond length: 2.130 Å
Largest bond length: 2.764 Å
Dopant-neighbor bond lengths (Zr–S): 2.558, 2.523, 2.558 Å

GaSe Nanoflake
Maximum diameter ($D_{\max}$): 13.217 Å
Corrugation: 0.000 Å
Radius of gyration (R_g): 5.270 Å
Average bond length: 2.470 Å
Smallest bond length: 2.259 Å
Largest bond length: 2.753 Å

GaSe:Mo Nanoflake
Maximum diameter ($D_{\max}$): 13.260 Å
Corrugation: 0.000 Å
Radius of gyration (R_g): 5.267 Å
Average bond length: 2.466 Å
Smallest bond length: 2.264 Å
Largest bond length: 2.786 Å
Dopant-neighbor bond lengths (Mo–Se): 2.527, 2.517, 2.527 Å

GaTe Nanoflake
Maximum diameter ($D_{\max}$): 14.075 Å
Corrugation: 0.000 Å
Radius of gyration (R_g): 5.656 Å
Average bond length: 2.659 Å
Smallest bond length: 2.455 Å
Largest bond length: 2.954 Å

GaTe:Mo Nanoflake
Maximum diameter ($D_{\max}$): 13.713 Å
Corrugation: 0.000 Å
Radius of gyration (R_g): 5.605 Å
Average bond length: 2.624 Å
Smallest bond length: 2.538 Å
Largest bond length: 2.750 Å
Dopant-neighbor bond lengths (Mo–Te): 2.750, 2.750, 2.750 Å

InS Nanoflake
Maximum diameter ($D_{\max}$): 13.631 Å
Corrugation: 0.000 Å
Radius of gyration (R_g): 5.369 Å
Average bond length: 2.495 Å
Smallest bond length: 2.293 Å
Largest bond length: 2.740 Å

InS:Zr Nanoflake
Maximum diameter ($D_{\max}$): 13.662 Å
Corrugation: 0.000 Å
Radius of gyration (R_g): 5.397 Å
Average bond length: 2.504 Å
Smallest bond length: 2.294 Å
Largest bond length: 2.750 Å
Dopant-neighbor bond lengths (Zr–S): 2.432, 2.432, 2.432 Å

InSe Nanoflake
Maximum diameter ($D_{\max}$): 14.128 Å
Corrugation: 0.000 Å
Radius of gyration (R_g): 5.627 Å
Average bond length: 2.628 Å
Smallest bond length: 2.421 Å
Largest bond length: 2.890 Å

InSe:Mo Nanoflake
Maximum diameter ($D_{\max}$): 13.740 Å
Corrugation: 0.000 Å
Radius of gyration (R_g): 5.526 Å
Average bond length: 2.585 Å
Smallest bond length: 2.483 Å
Largest bond length: 2.733 Å
Dopant-neighbor bond lengths (Mo–Se): 2.663, 2.637, 2.636 Å

InTe Nanoflake
Maximum diameter ($D_{\max}$): 14.990 Å
Corrugation: 0.000 Å
Radius of gyration (R_g): 6.017 Å
Average bond length: 2.822 Å
Smallest bond length: 2.609 Å
Largest bond length: 3.113 Å

InTe:Mo Nanoflake
Maximum diameter ($D_{\max}$): 14.451 Å
Corrugation: 0.000 Å
Radius of gyration (R_g): 5.895 Å
Average bond length: 2.768 Å
Smallest bond length: 2.691 Å
Largest bond length: 2.874 Å
Dopant-neighbor bond lengths (Mo–Te): 2.788, 2.788, 2.788 Å

TlS Nanoflake
Maximum diameter ($D_{\max}$): 14.292 Å
Corrugation: 0.000 Å
Radius of gyration (R_g): 5.646 Å
Average bond length: 2.625 Å
Smallest bond length: 2.406 Å
Largest bond length: 2.891 Å

TlS:Mn Nanoflake
Maximum diameter ($D_{\max}$): 14.298 Å
Corrugation: 0.000 Å
Radius of gyration (R_g): 5.517 Å
Average bond length: 2.587 Å
Smallest bond length: 2.391 Å
Largest bond length: 2.920 Å
Dopant-neighbor bond lengths (Mn–S): 2.391, 2.449, 2.391 Å

TlSe Nanoflake
Maximum diameter ($D_{\max}$): 14.748 Å
Corrugation: 0.000 Å
Radius of gyration (R_g): 5.888 Å
Average bond length: 2.748 Å
Smallest bond length: 2.530 Å
Largest bond length: 3.022 Å

TlSe:Mn Nanoflake
Maximum diameter ($D_{\max}$): 14.585 Å
Corrugation: 0.000 Å
Radius of gyration (R_g): 5.756 Å
Average bond length: 2.709 Å
Smallest bond length: 2.495 Å
Largest bond length: 3.029 Å
Dopant-neighbor bond lengths (Mn–Se): 2.525, 2.495, 2.525 Å

TlTe Nanoflake
Maximum diameter ($D_{\max}$): 15.586 Å
Corrugation: 0.000 Å
Radius of gyration (R_g): 6.269 Å
Average bond length: 2.937 Å
Smallest bond length: 2.715 Å
Largest bond length: 3.236 Å

TlTe:Mn Nanoflake
Maximum diameter ($D_{\max}$): 15.950 Å
Corrugation: 0.000 Å
Radius of gyration (R_g): 6.174 Å
Average bond length: 2.912 Å
Smallest bond length: 2.670 Å
Largest bond length: 3.269 Å
Dopant-neighbor bond lengths (Mn–Te): 2.671, 2.693, 2.670 Å

3 Formation Energies of Charged States

Table S1: Formation energies, energy differences, and spin states of the considered structures in their charged configurations.

Host	**Dp**	$E_{\text{form}}^{(q)}$ (eV)	ΔE (eV)	M
Ga_9S_{12}	Zr	-3.14	+1.64	6
Ga_9Se_{12}	Mo	-6.01	-1.11	6
Ga_9Te_{12}	Mo	-6.11	-1.57	6
In_9S_{12}	Zr	-2.97	+2.20	4
In_9Se_{12}	Mo	-6.01	-1.27	6
In_9Te_{12}	Mo	-6.12	-1.24	6
Tl_9S_{12}	Mn	-4.70	+0.14	7
Tl_9Se_{12}	Mn	-3.76	+0.44	9
Tl_9Te_{12}	Mn	-3.46	+1.16	7

We have computed the formation energies of the pristine and TM-substituted structures in multiple charge states, specifically $q = \pm 1$ and $q = \pm 2$. For $q = \pm 1$, the system adopts the spin of the charged state, whereas for $q = \pm 2$, the original spin configuration of the neutral system is preserved. We find that the anionic state with $q = -2$ exhibits the lowest formation energy for both pristine and doped systems. The charged state formation energy ($E_{\text{form}}^{(q)}$) is defined as:

$$E_{\text{form}}^{-2} = E^{-2}(\text{M}_9\text{TMX}_{12}) - E^{-2}(\text{M}_{10}\text{X}_{12}) + \mu_M - \mu_{\text{TM}} \tag{7}$$

where $E^{-2}(\text{M}_9\text{TMX}_{12})$ is the total energy of the doped system at charge -2,
$E^{-2}(\text{M}_{10}\text{X}_{12})$ is the total energy of the pristine system at charge -2,
μ_M is the chemical potential of the removed host atom, and
μ_{TM} is the chemical potential of the inserted dopant atom.

As presented in Table **S1**, $E_{\text{form}}^{(q)}$ increases by 1.11, 1.57, 1.27, and 1.24 eV for Ga_9MoSe_{12}, Ga_9MoTe_{12}, In_9MoSe_{12}, and In_9MoTe_{12}, respectively, whereas it decreases for the rest compared to the neutral states. Larger spin differences relative to the neutral system are observed for Ga_9ZrS_{12} (sextet), In_9ZrS_{12} (quartet), Tl_9MnSe_{12} (nonet), and Tl_9MnTe_{12} (septet); however, these differences do not qualitatively affect the observed stability trends. Furthermore, Mulliken population analysis of the anionic systems (presented in Table **S13 – S21**) shows that substitutional transition-metal dopants (Zr, Mo, Mn) adopt lower effective charges than host cations and carry dominant spin densities ($\sim 1.9 - 4.8\mu_B$), which indicates strong localization of unpaired d-electrons at the dopant sites. The surrounding atoms exhibit noticeable changes in charge and spin density, confirming that single-site perturbation modifies the local electronic structure of the quantum dots.

4 Charge Distribution Anisotropy

Table S2: Traceless quadrupole tensor components of the quantum dots in atomic units (1 a.u. = 4.486551 Debye·Å).

System	Q_{xx}	Q_{yy}	Q_{zz}	Q_{xy}	Q_{xz}	Q_{yz}
$Ga_{10}S_{12}$	10.1725	−5.0844	−5.0880	0.0000	0.0000	0.0000
Ga_9ZrS_{12}	8.2539	−10.1990	1.9451	0.0000	0.0000	0.0000
$Ga_{10}Se_{12}$	8.9102	−4.4685	−4.4418	0.0000	0.0000	0.0000
Ga_9MoSe_{12}	7.5705	−9.3135	1.7430	0.0000	0.0000	0.0000
$Ga_{10}Te_{12}$	6.5891	−3.2894	−3.2997	0.0000	0.0000	0.0000
Ga_9MoTe_{12}	4.0811	−2.0171	−2.0640	0.0000	0.0000	0.0000
$In_{10}S_{12}$	−6.7482	−6.7669	13.5152	−0.0062	0.0000	0.0000
In_9ZrS_{12}	−6.4365	−6.4564	12.8929	−0.0033	0.0000	0.0000
$In_{10}Se_{12}$	−5.9712	−5.9050	11.8762	−0.0032	0.0000	0.0000
In_9MoSe_{12}	−7.3918	−0.4096	7.8014	−0.1254	0.0000	0.0000
$In_{10}Te_{12}$	−4.4548	−4.4836	8.9383	−0.0152	0.0000	0.0000
In_9MoTe_{12}	−2.8925	−2.8620	5.7545	−0.0385	0.0000	0.0000
$Tl_{10}S_{12}$	−85.1527	−85.1069	−75.4043	−0.0192	0.0000	0.0000
Tl_9MnS_{12}	−8.7045	2.9022	5.8023	−0.0325	0.0000	0.0000
$Tl_{10}Se_{12}$	5.2459	−2.7170	−2.5289	0.0000	0.0000	0.0000
Tl_9MnSe_{12}	4.4097	−0.5362	−3.8735	0.0000	0.0000	0.0000
$Tl_{10}Te_{12}$	−1.2167	−1.1672	2.3839	−0.0282	0.0000	0.0000
Tl_9MnTe_{12}	−8.6956	12.0515	−3.3559	0.0205	0.0000	0.0000

Supplementary Notes

To capture the spatial anisotropy of electron density distribution in the nanoflakes, we calculated the traceless quadrupole tensor components, to identify higher-order deviations from spherical symmetry. As given in Table **S2**, data from quadrupole moments showing how the electron cloud is stretched or compressed along specific Cartesian directions, from which we can characterize directional polarization patterns that were not apparent in dipole analysis alone. The sum over all components would be zero, and the positive or negative value explains how the density spreads or contracts in each principle axis. For the pristine $Ga_{10}X_{12}$ configurations, the elongation or distribution is more diffuse along the x-axis, while $In_{10}X_{12}$ and $Tl_{10}X_{12}$ primarily showed compression in the in-plane-axis. Particularly, $Tl_{10}S_{12}$ shows huge contraction of wavefunctions most likely due to higher localization of *s*-orbitals just above the Fermi level (being non-directional but energetically accessible), which creates such concentration in real space. The distribution is then extends in the out-of-plane direction for most of the nanodots after substitution with TM.

5 Cross-spin's Non-orthogonality

Table S3: Cross-spin overlap integrals and normalized overlaps for all systems.

System	Overlap pair	Overlap integral	Normalized overlap
Ga_9ZrS_{12}	Hα–Hβ	5.0684×10^{-2}	0.050700
	Lα–Lβ	2.0665×10^{-1}	0.207050
Ga_9MoSe_{12}	Hα–Hβ	9.9927×10^{-1}	0.999907
	Lα–Lβ	-6.1680×10^{-8}	0.000000
Ga_9MoTe_{12}	Hα–Hβ	-9.5054×10^{-4}	0.000951
	Lα–Lβ	1.3611×10^{-1}	0.136262
In_9ZrS_{12}	Hα–Hβ	9.9880×10^{-1}	0.999999
	Lα–Lβ	3.7337×10^{-3}	0.003770
In_9MoSe_{12}	Hα–Hβ	-5.0716×10^{-2}	0.050770
	Lα–Lβ	-2.9780×10^{-4}	0.000298
In_9MoTe_{12}	Hα–Hβ	1.1492×10^{-3}	0.001151
	Lα–Lβ	9.0809×10^{-4}	0.000910
Tl_9MnS_{12}	Hα–Hβ	9.9863×10^{-1}	0.999421
	Lα–Lβ	1.9058×10^{-1}	0.190898
Tl_9MnSe_{12}	Hα–Hβ	-2.6589×10^{-1}	0.266197
	Lα–Lβ	1.7976×10^{-6}	0.000002
Tl_9MnTe_{12}	Hα–Hβ	9.9477×10^{-1}	0.995865
	Lα–Lβ	2.4923×10^{-4}	0.000250

6 Element-Projected Partial Density of States

Figure S1. Element-projected partial density of states plotted for the pristine and doped configurations comprises the total contribution from each group of atoms. The TM-X_3 hybridization strength vastly depends on the host structure. Moreover, electronic contribution from the host-metal (Ga, In) reduces upon dopant incorporation, whereas in Tl-based systems, the host metal remains dominant, that contributes a major portion of the states near the Fermi level.

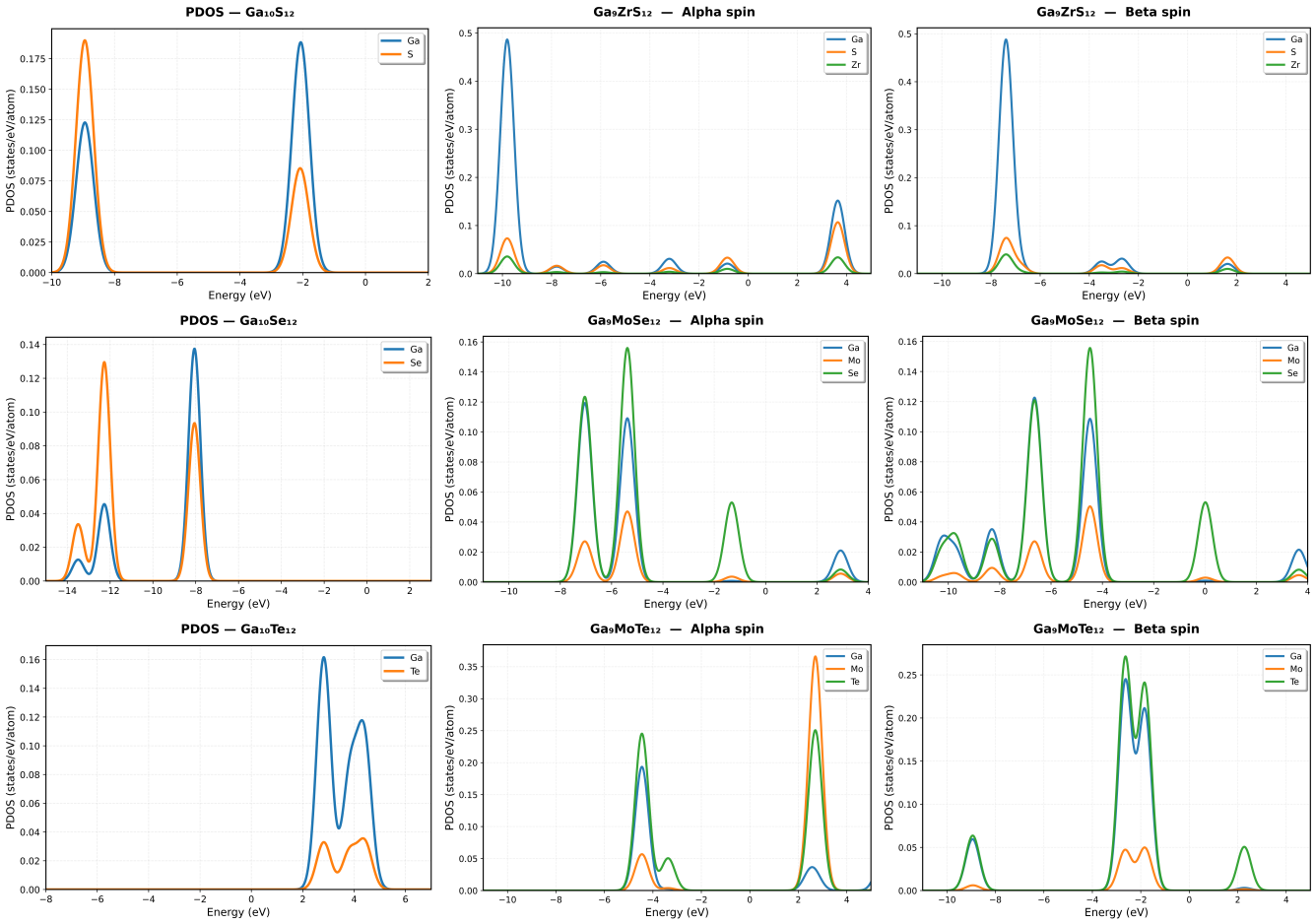

Figure S1(a): Element-projected PDOS for Ga-based systems. The plots correspond to pristine $Ga_{10}X_{12}$, Zr-doped Ga_9S_{12}, and Mo-doped $Ga_9(Se/Te)_{12}$ configurations. Specific compositions are indicated within each panel.

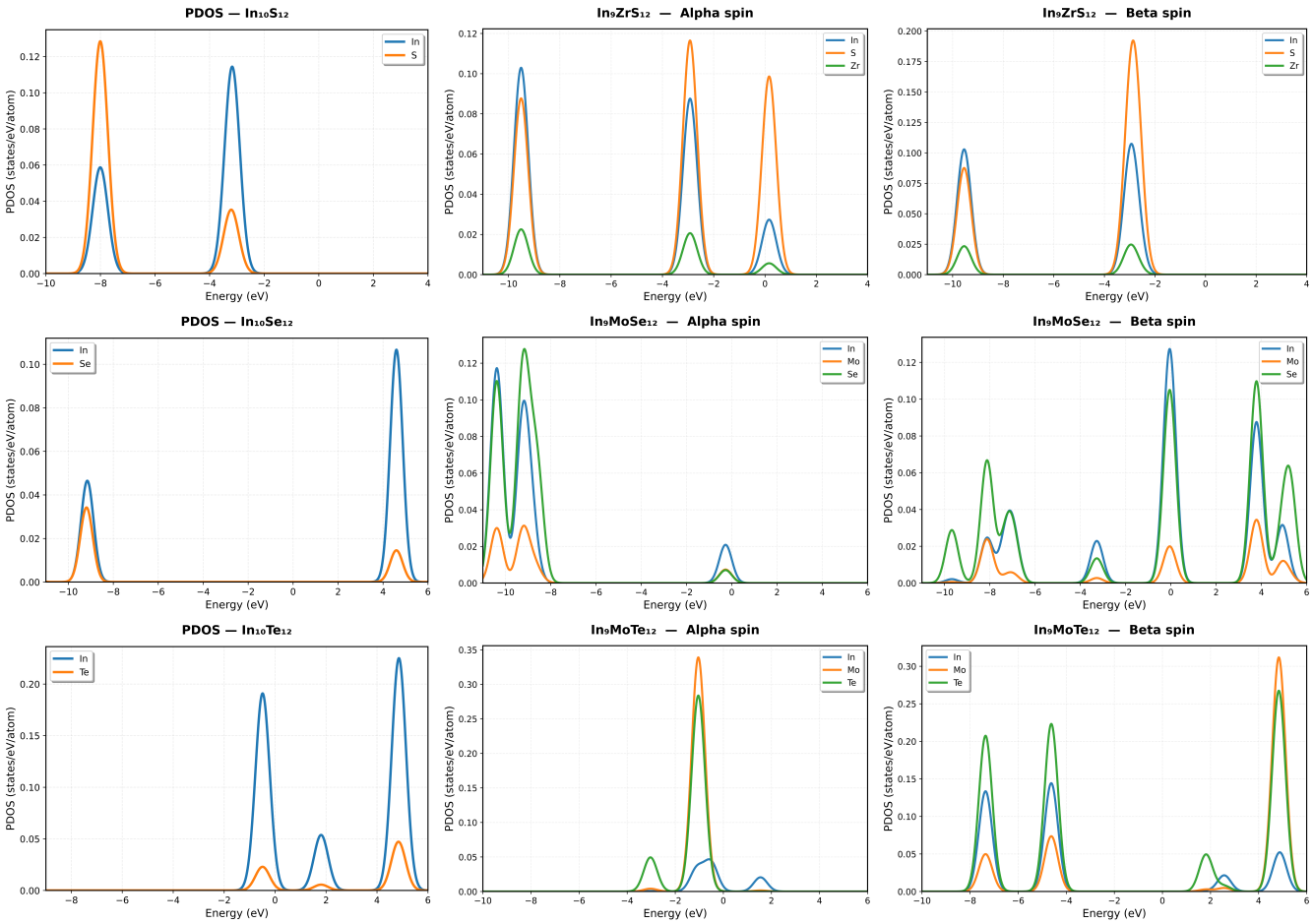

Figure S1(b): Element-projected PDOS for In-based systems. The plots correspond to pristine $In_{10}X_{12}$, Zr-doped In_9S_{12}, and Mo-doped $In_9(Se/Te)_{12}$ configurations. Specific compositions are indicated within each panel.

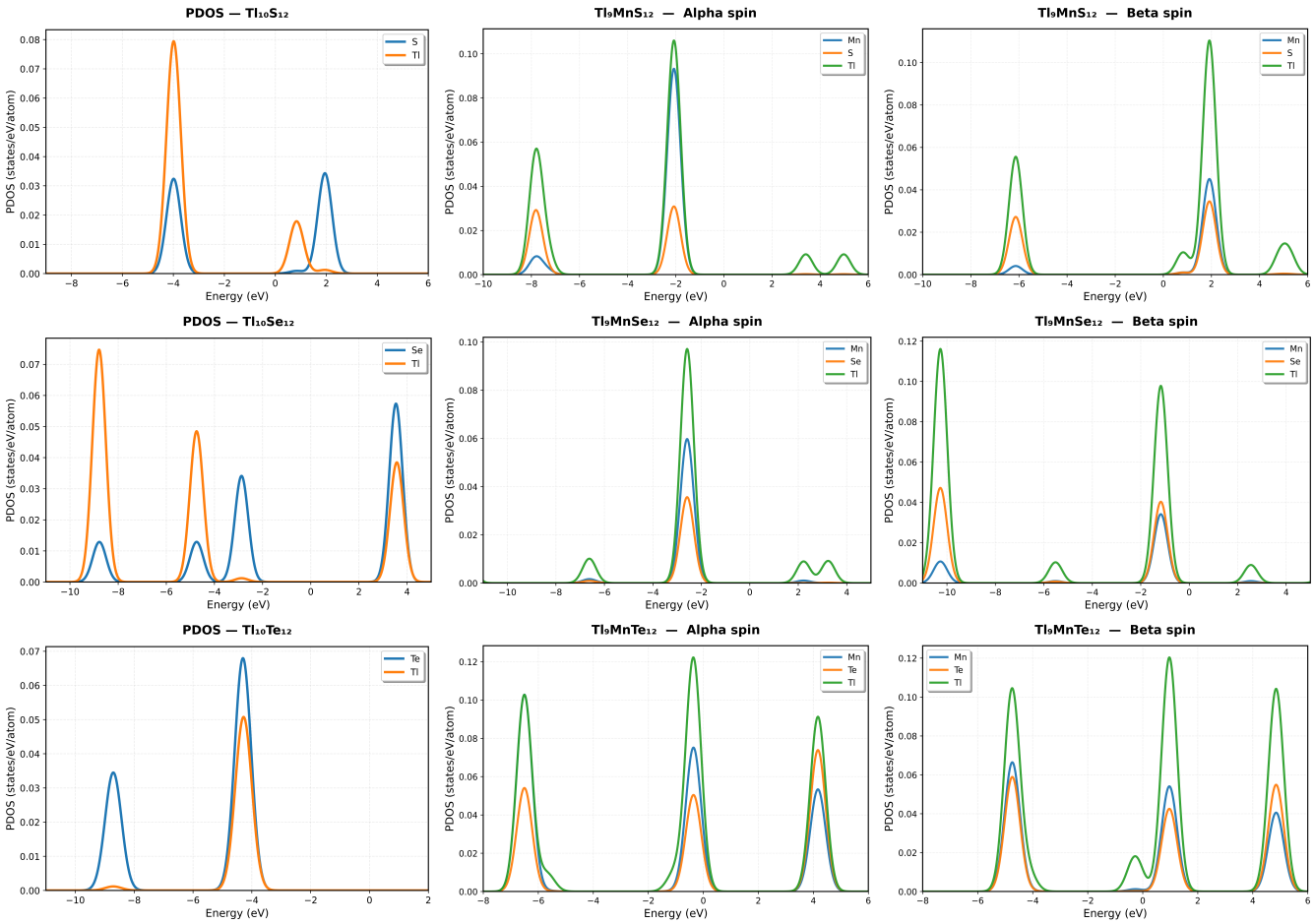

Figure S1(c): Element-projected PDOS for Tl-based systems. The plots correspond to pristine $Tl_{10}X_{12}$, and Mn-doped $Tl_9(S/Se/Te)_{12}$ configurations. Specific compositions are indicated within each panel.

Supplementary Notes

The element-projected PDOS provides a more detail look on understanding at how each group of atoms contributes to the potential landscape. In Mo-doped Ga_9Te_{12} and In_9Te_{12}, we can see that intensity from the dopant is high compared to other configurations. This is a key factor that leads to higher distribution of spin density in the configurations. But in case of Mn-substituted Tl_9X_{12} configurations, the reduced orbital intensity from the dopant disrupts local symmetry, which results in non-uniform orbital distributions, a large nonlinear response, and phase inversion behavior.

7 Total Density of States

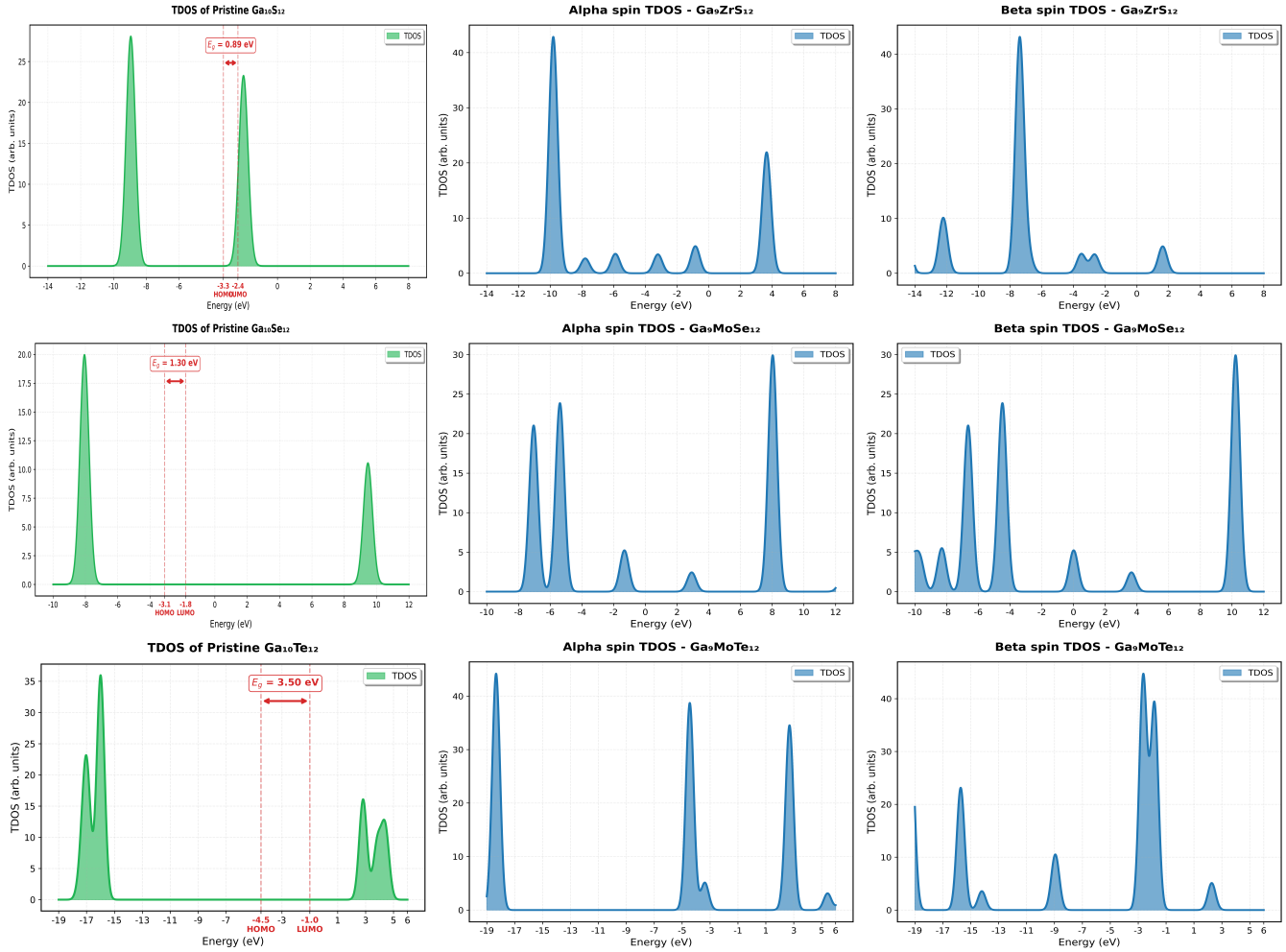

Figure S2(a):

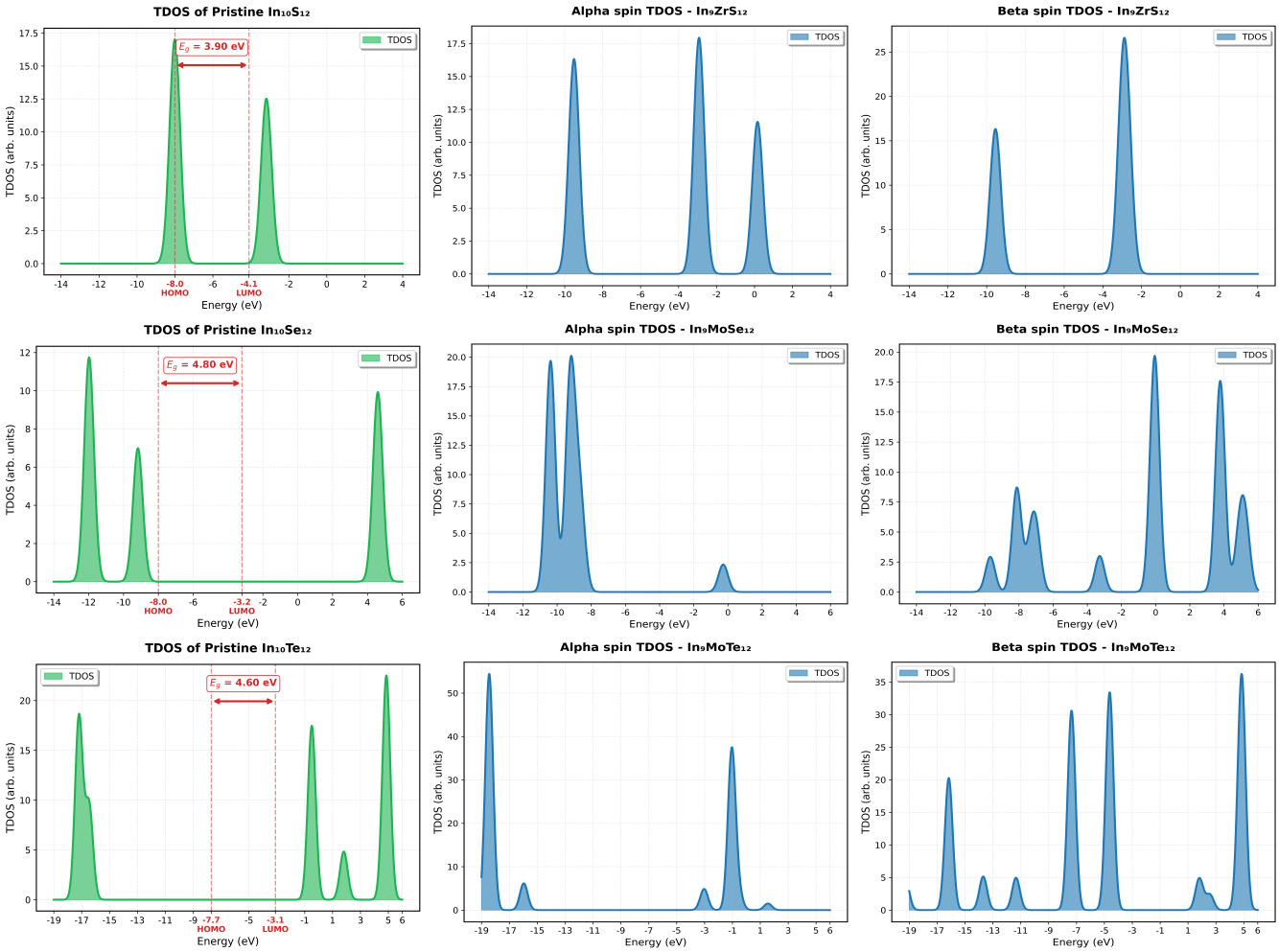
TDOS of Pristine In10S12
Eg = 3.90 eV
-8.0 HOMO
-4.1 LUMO
Alpha spin TDOS - In9ZrS12
Beta spin TDOS - In9ZrS12
TDOS of Pristine In10Se12
Eg = 4.80 eV
-8.0 HOMO
-3.2 LUMO
Alpha spin TDOS - In9MoSe12
Beta spin TDOS - In9MoSe12
TDOS of Pristine In10Te12
Eg = 4.60 eV
-7.7 HOMO
-3.1 LUMO
Alpha spin TDOS - In9MoTe12
Beta spin TDOS - In9MoTe12
TDOS
TDOS (arb. units)
Energy (eV)

Figure S2(b):

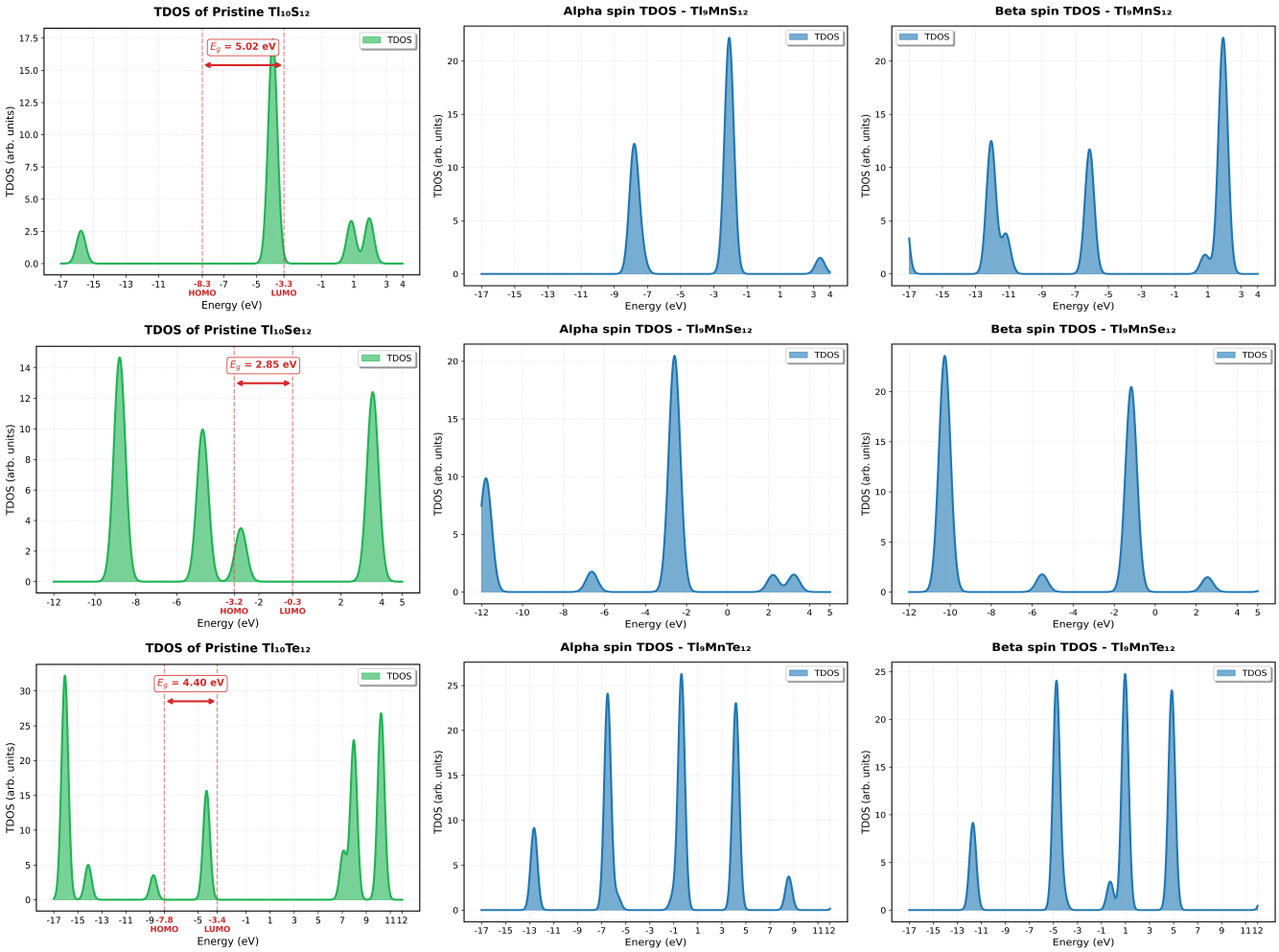
TDOS of Pristine Tl10S12
Alpha spin TDOS - Tl9MnS12
Beta spin TDOS - Tl9MnS12
TDOS of Pristine Tl10Se12
Alpha spin TDOS - Tl9MnSe12
Beta spin TDOS - Tl9MnSe12
TDOS of Pristine Tl10Te12
Alpha spin TDOS - Tl9MnTe12
Beta spin TDOS - Tl9MnTe12
TDOS
TDOS (arb. units)
Energy (eV)
Eg = 5.02 eV
-8.3 HOMO
-3.3 LUMO
Eg = 2.85 eV
-3.2 HOMO
-0.3 LUMO
Eg = 4.40 eV
-7.8 HOMO
-3.4 LUMO

Figure S2(c):

8 Mulliken Atomic Charges and Spin Populations of the Studied Configurations

Mulliken population analysis is used here as a qualitative indicator of charge redistribution and spin localization, that supports the real-space orbital and spin-density visualizations. The Mulliken charge and spin-density analysis exhibits that pristine group-13 chalcogenide quantum dots shows a systematic reduction in ionicity from S to Te. This indicates an increment in more covalence-like behavior and electronic softness of the host framework. Upon transition-metal doping, the dopant atom acquires partial positive charge and is the main source of magnetic moments in the electronic structure. Such center-substitution causes partial charge transfer, higher covalent hybridization, and high spin polarization on neighboring host atoms. It is also observed that, when the host structure contains heavier chalcogen, the delocalization of spin redistribution increases (because their orbitals are more diffuse, as per Fig. S1) due to the enhanced p–d hybridization and spin-selective charge rehybridization. Moreover, presence of dopant changes the local charge distribution as some of the host atoms become less negative (or more positive), which indicates charge reorganizations in the configuration. It is also evident that some host atoms gain spin but a minor change in electronic charge is observed, which suggests that spin-selective charge rehybridization becomes much higher in heavier chalcogen hosts due to their increased electronic softness. It is also observed from our analysis that while the dopant identity controls the magnitude of magnetization, the host orbital-interaction governs its spatial extent (i.e., distribution), which establishes a clear structure-property relationship for tuning magnetism in such low-dimensional systems.

Table S4: Mulliken charges for pristine $Ga_{10}S_{12}$ QD (Table A) and Zr-doped Ga_9S_{12} QD (Table B) with spin densities.

Atom	Pristine (A)		Doped (B)		
	Element	Charge (e)	Element	Charge (e)	Spin Density (μ_B)
1	Ga	0.708	Ga	0.697	0.016
2	S	-0.688	S	-0.731	-0.027
3	Ga	0.708	Ga	0.745	0.021
4	S	-0.540	S	-0.524	0.014
5	Ga	0.516	Ga	0.503	0.001
6	S	-0.540	S	-0.560	0.010
7	S	-0.486	S	-0.716	-0.025
8	Ga	0.708	Ga	0.745	0.021
9	S	-0.688	S	-0.731	-0.027
10	Ga	0.963	Zr	1.076	1.935
11	Ga	0.708	Ga	0.697	0.016
12	S	-0.540	S	-0.560	0.010
13	Ga	0.516	Ga	0.503	0.001
14	S	-0.540	S	-0.524	0.014
15	S	-0.485	S	-0.486	0.017
16	Ga	0.708	Ga	0.751	0.035
17	S	-0.688	S	-0.759	-0.027
18	S	-0.485	S	-0.486	0.017
19	Ga	0.708	Ga	0.751	0.035
20	S	-0.540	S	-0.475	0.106
21	Ga	0.516	Ga	0.562	0.733
22	S	-0.540	S	-0.475	0.106

Table S5: Mulliken charges for pristine $Ga_{10}Se_{12}$ QD (Table A) and Mo-doped Ga_9Se_{12} QD (Table B) with spin densities.

Atom	Pristine (A)		Doped (B)		
	Element	Charge (e)	Element	Charge (e)	Spin Density (μ_B)
1	Ga	0.547	Ga	0.523	0.014
2	Se	-0.562	Se	-0.513	-0.012
3	Ga	0.547	Ga	0.544	0.011
4	Se	-0.458	Se	-0.479	0.014
5	Ga	0.443	Ga	0.419	0.001
6	Se	-0.458	Se	-0.455	0.008
7	Se	-0.320	Se	-0.348	0.015
8	Ga	0.547	Ga	0.544	0.011
9	Se	-0.562	Se	-0.513	-0.012
10	Ga	0.784	Mo	0.687	3.838
11	Ga	0.547	Ga	0.523	0.014
12	Se	-0.458	Se	-0.455	0.008
13	Ga	0.443	Ga	0.419	0.001
14	Se	-0.458	Se	-0.479	0.014
15	Se	-0.319	Se	-0.351	0.014
16	Ga	0.547	Ga	0.568	0.022
17	Se	-0.562	Se	-0.625	0.069
18	Se	-0.319	Se	-0.351	0.014
19	Ga	0.547	Ga	0.568	0.022
20	Se	-0.458	Se	-0.343	0.139
21	Ga	0.443	Ga	0.460	0.656
22	Se	-0.458	Se	-0.343	0.139

Table S6: Mulliken charges for pristine $Ga_{10}Te_{12}$ QD (Table A) and Mo-doped Ga_9Te_{12} QD (Table B) with spin densities.

Atom	Pristine (A)		Doped (B)		
	Element	Charge (e)	Element	Charge (e)	Spin Density (μ_B)
1	Ga	0.258	Ga	0.255	0.017
2	Te	-0.352	Te	-0.321	0.010
3	Ga	0.257	Ga	0.255	0.017
4	Te	-0.302	Te	-0.214	0.151
5	Ga	0.356	Ga	0.268	0.408
6	Te	-0.302	Te	-0.214	0.150
7	Te	-0.074	Te	-0.136	0.013
8	Ga	0.257	Ga	0.255	0.017
9	Te	-0.352	Te	-0.321	0.010
10	Ga	0.475	Mo	0.323	4.707
11	Ga	0.258	Ga	0.255	0.017
12	Te	-0.302	Te	-0.214	0.150
13	Ga	0.356	Ga	0.268	0.408
14	Te	-0.302	Te	-0.214	0.151
15	Te	-0.073	Te	-0.136	0.013
16	Ga	0.257	Ga	0.254	0.017
17	Te	-0.351	Te	-0.319	0.009
18	Te	-0.073	Te	-0.136	0.013
19	Ga	0.257	Ga	0.254	0.017
20	Te	-0.302	Te	-0.213	0.149
21	Ga	0.356	Ga	0.267	0.410
22	Te	-0.302	Te	-0.213	0.149

Table S7: Mulliken charges for pristine $In_{10}S_{12}$ QD (Table A) and Zr-doped In_9S_{12} QD (Table B) with spin densities.

Atom	Pristine (A)		Doped (B)		
	Element	Charge (e)	Element	Charge (e)	Spin Density (μ_B)
1	In	0.857	In	0.848	0.000
2	S	-0.780	S	-0.782	-0.014
3	In	0.857	In	0.848	0.000
4	S	-0.618	S	-0.615	-0.001
5	In	0.550	In	0.549	0.000
6	S	-0.618	S	-0.615	-0.001
7	S	-0.614	S	-0.626	0.001
8	In	0.857	In	0.848	0.000
9	S	-0.780	S	-0.782	-0.014
10	In	1.101	Zr	1.177	1.048
11	In	0.857	In	0.848	0.000
12	S	-0.618	S	-0.615	-0.001
13	In	0.550	In	0.549	0.000
14	S	-0.619	S	-0.615	-0.001
15	S	-0.614	S	-0.626	0.001
16	In	0.857	In	0.848	0.000
17	S	-0.780	S	-0.782	-0.014
18	S	-0.614	S	-0.626	0.001
19	In	0.857	In	0.848	0.000
20	S	-0.618	S	-0.615	-0.001
21	In	0.550	In	0.549	0.000
22	S	-0.618	S	-0.615	-0.001

Table S8: Mulliken charges for pristine $In_{10}Se_{12}$ QD (Table A) and Mo-doped In_9Se_{12} QD (Table B) with spin densities.

Atom	Pristine (A)		Doped (B)		
	Element	Charge (e)	Element	Charge (e)	Spin Density (μ_B)
1	In	0.689	In	0.687	0.027
2	Se	-0.664	Se	-0.661	-0.003
3	In	0.689	In	0.681	-0.020
4	Se	-0.532	Se	-0.491	0.142
5	In	0.492	In	0.484	0.322
6	Se	-0.531	Se	-0.496	0.111
7	Se	-0.448	Se	-0.465	0.014
8	In	0.689	In	0.681	-0.019
9	Se	-0.664	Se	-0.661	-0.003
10	In	0.918	Mo	0.581	4.756
11	In	0.688	In	0.687	0.027
12	Se	-0.531	Se	-0.496	0.110
13	In	0.492	In	0.484	0.322
14	Se	-0.531	Se	-0.492	0.142
15	Se	-0.448	Se	-0.453	0.020
16	In	0.689	In	0.703	0.035
17	Se	-0.664	Se	-0.664	-0.007
18	Se	-0.452	Se	-0.452	0.020
19	In	0.703	In	0.703	0.035
20	Se	-0.447	Se	-0.447	0.182
21	In	0.535	In	0.534	0.605
22	Se	-0.447	Se	-0.447	0.182

Table S9: Mulliken charges for pristine $In_{10}Te_{12}$ QD (Table A) and Mo-doped In_9Te_{12} QD (Table B) with spin densities.

Atom	Pristine (A)		Doped (B)		
	Element	Charge (e)	Element	Charge (e)	Spin Density (μ_B)
1	In	0.435	In	0.424	0.014
2	Te	-0.481	Te	-0.431	-0.001
3	In	0.435	In	0.424	0.014
4	Te	-0.404	Te	-0.327	0.164
5	In	0.433	In	0.375	0.388
6	Te	-0.404	Te	-0.326	0.164
7	Te	-0.224	Te	-0.260	0.013
8	In	0.435	In	0.424	0.015
9	Te	-0.481	Te	-0.431	-0.001
10	In	0.632	Mo	0.360	4.731
11	In	0.435	In	0.424	0.014
12	Te	-0.404	Te	-0.326	0.164
13	In	0.432	In	0.375	0.389
14	Te	-0.404	Te	-0.326	0.164
15	Te	-0.225	Te	-0.260	0.012
16	In	0.425	In	0.425	0.014
17	Te	-0.481	Te	-0.431	-0.001
18	Te	-0.224	Te	-0.260	0.012
19	In	0.425	In	0.425	0.014
20	Te	-0.404	Te	-0.326	0.164
21	In	0.433	In	0.375	0.389
22	Te	-0.404	Te	-0.326	0.163

Table S10: Mulliken charges for pristine $Tl_{10}S_{12}$ QD (Table A) and Mn-doped Tl_9S_{12} QD (Table B) with spin densities.

Atom	Pristine (A)		Doped (B)		
	Element	Charge (e)	Element	Charge (e)	Spin Density (μ_B)
1	Tl	0.818	Tl	0.810	-0.001
2	S	-0.768	S	-0.768	0.057
3	Tl	0.817	Tl	0.805	0.001
4	S	-0.616	S	-0.598	0.023
5	Tl	0.630	Tl	0.612	0.000
6	S	-0.617	S	-0.645	0.011
7	S	-0.590	S	-0.544	0.031
8	Tl	0.818	Tl	0.831	-0.004
9	S	-0.768	S	-0.771	0.028
10	Tl	0.974	Mn	0.751	4.742
11	Tl	0.818	Tl	0.831	-0.003
12	S	-0.617	S	-0.545	0.315
13	Tl	0.631	Tl	0.690	0.357
14	S	-0.616	S	-0.545	0.315
15	S	-0.589	S	-0.586	0.006
16	Tl	0.818	Tl	0.810	-0.001
17	S	-0.768	S	-0.768	0.058
18	S	-0.590	S	-0.544	0.031
19	Tl	0.818	Tl	0.805	0.001
20	S	-0.617	S	-0.598	0.023
21	Tl	0.632	Tl	0.612	0.000
22	S	-0.617	S	-0.645	0.011

Table S11: Mulliken charges for pristine $Tl_{10}Se_{12}$ QD (Table A) and Mn-doped Tl_9Se_{12} QD (Table B) with spin densities.

Atom	Pristine (A)		Doped (B)		
	Element	Charge (e)	Element	Charge (e)	Spin Density (μ_B)
1	Tl	0.690	Tl	0.695	0.005
2	Se	-0.676	Se	-0.666	0.041
3	Tl	0.690	Tl	0.665	-0.034
4	Se	-0.549	Se	-0.458	0.344
5	Tl	0.579	Tl	0.583	0.115
6	Se	-0.549	Se	-0.558	0.066
7	Se	-0.463	Se	-0.409	0.075
8	Tl	0.690	Tl	0.665	-0.034
9	Se	-0.676	Se	-0.666	0.041
10	Tl	0.835	Mn	0.663	4.731
11	Tl	0.690	Tl	0.695	0.005
12	Se	-0.549	Se	-0.558	0.066
13	Tl	0.579	Tl	0.583	0.115
14	Se	-0.549	Se	-0.458	0.344
15	Se	-0.464	Se	-0.458	0.012
16	Tl	0.689	Tl	0.684	0.001
17	Se	-0.676	Se	-0.678	0.058
18	Se	-0.464	Se	-0.458	0.012
19	Tl	0.689	Tl	0.684	0.001
20	Se	-0.549	Se	-0.553	0.019
21	Tl	0.581	Tl	0.562	-0.001
22	Se	-0.549	Se	-0.553	0.019

Table S12: Mulliken charges for pristine $Tl_{10}Te_{12}$ QD (Table A) and Mn-doped Tl_9Te_{12} QD (Table B) with spin densities.

Atom	Pristine (A)		Doped (B)		
	Element	Charge (e)	Element	Charge (e)	Spin Density (μ_B)
1	Tl	0.499	Tl	0.498	0.000
2	Te	-0.548	Te	-0.483	0.044
3	Tl	0.499	Tl	0.491	0.003
4	Te	-0.452	Te	-0.456	0.019
5	Tl	0.538	Tl	0.524	-0.002
6	Te	-0.453	Te	-0.477	0.014
7	Te	-0.293	Te	-0.285	0.026
8	Tl	0.498	Tl	0.535	0.027
9	Te	-0.547	Te	-0.451	0.027
10	Tl	0.626	Mn	0.332	4.742
11	Tl	0.499	Tl	0.536	0.027
12	Te	-0.453	Te	-0.456	-0.533
13	Tl	0.539	Tl	0.661	0.028
14	Te	-0.453	Te	-0.456	-0.534
15	Te	-0.292	Te	-0.322	0.008
16	Tl	0.498	Tl	0.498	0.000
17	Te	-0.547	Te	-0.483	0.044
18	Te	-0.293	Te	-0.285	0.026
19	Tl	0.499	Tl	0.491	0.003
20	Te	-0.452	Te	-0.456	0.019
21	Tl	0.539	Tl	0.523	-0.002
22	Te	-0.453	Te	-0.477	0.014

Mulliken Population Analysis of Anionic Pristine and Transition-Metal-Doped PTMC Quantum Dots

Table S13: Mulliken charges for pristine $Ga_{10}S_{12}$ QD (Table A) and Zr-doped Ga_9S_{12} QD (Table B) with spin densities.

Atom	Pristine (A)		Doped (B)		
	Element	Charge (e)	Element	Charge (e)	Spin Density (μ_B)
1	Ga	0.680	Ga	0.628	0.017
2	S	-0.705	S	-0.687	-0.021
3	Ga	0.680	Ga	0.695	0.021
4	S	-0.624	S	-0.595	0.012
5	Ga	0.344	Ga	0.353	0.002
6	S	-0.624	S	-0.669	0.010
7	S	-0.615	S	-0.738	-0.018
8	Ga	0.680	Ga	0.695	0.021
9	S	-0.705	S	-0.687	-0.021
10	Ga	0.590	Zr	0.865	1.971
11	Ga	0.680	Ga	0.628	0.017
12	S	-0.624	S	-0.669	0.010
13	Ga	0.344	Ga	0.353	0.002
14	S	-0.624	S	-0.595	0.012
15	S	-0.615	S	-0.549	0.130
16	Ga	0.680	Ga	0.540	0.701
17	S	-0.705	S	-0.727	0.106
18	S	-0.615	S	-0.549	0.130
19	Ga	0.680	Ga	0.540	0.701
20	S	-0.624	S	-0.581	0.247
21	Ga	0.343	Ga	0.328	0.702
22	S	-0.624	S	-0.581	0.247

Table S14: Mulliken charges for pristine $Ga_{10}Se_{12}$ QD (Table A) and Mo-doped Ga_9Se_{12} QD (Table B) with spin densities.

Atom	Pristine (A)		Doped (B)		
	Element	Charge (e)	Element	Charge (e)	Spin Density (μ_B)
1	Ga	0.535	Ga	0.521	0.023
2	Se	-0.605	Se	-0.576	0.007
3	Ga	0.536	Ga	0.521	0.023
4	Se	-0.554	Se	-0.555	0.017
5	Ga	0.280	Ga	0.271	-0.001
6	Se	-0.554	Se	-0.556	0.017
7	Se	-0.485	Se	-0.460	0.002
8	Ga	0.536	Ga	0.521	0.023
9	Se	-0.605	Se	-0.576	0.007
10	Ga	0.537	Mo	0.502	4.737
11	Ga	0.535	Ga	0.521	0.023
12	Se	-0.554	Se	-0.556	0.017
13	Ga	0.280	Ga	0.271	-0.001
14	Se	-0.554	Se	-0.555	0.017
15	Se	-0.485	Se	-0.460	0.002
16	Ga	0.536	Ga	0.521	0.023
17	Se	-0.605	Se	-0.576	0.007
18	Se	-0.485	Se	-0.460	0.002
19	Ga	0.536	Ga	0.521	0.023
20	Se	-0.554	Se	-0.555	0.017
21	Ga	0.280	Ga	0.271	-0.001
22	Se	-0.554	Se	-0.555	0.017

Table S15: Mulliken charges for pristine $Ga_{10}Te_{12}$ QD (Table A) and Mo-doped Ga_9Te_{12} QD (Table B) with spin densities.

Atom	Pristine (A)		Doped (B)		
	Element	Charge (e)	Element	Charge (e)	Spin Density (μ_B)
1	Ga	0.269	Ga	0.249	0.022
2	Te	-0.425	Te	-0.324	0.006
3	Ga	0.269	Ga	0.249	0.022
4	Te	-0.427	Te	-0.431	0.022
5	Ga	0.205	Ga	0.192	-0.002
6	Te	-0.427	Te	-0.431	0.022
7	Te	-0.287	Te	-0.250	0.003
8	Ga	0.269	Ga	0.249	0.022
9	Te	-0.425	Te	-0.324	0.006
10	Ga	0.467	Mo	0.240	4.716
11	Ga	0.269	Ga	0.249	0.022
12	Te	-0.427	Te	-0.431	0.022
13	Ga	0.205	Ga	0.192	-0.002
14	Te	-0.427	Te	-0.431	0.022
15	Te	-0.287	Te	-0.250	0.003
16	Ga	0.269	Ga	0.248	0.022
17	Te	-0.425	Te	-0.324	0.006
18	Te	-0.287	Te	-0.250	0.003
19	Ga	0.269	Ga	0.248	0.022
20	Te	-0.427	Te	-0.430	0.022
21	Ga	0.205	Ga	0.192	-0.002
22	Te	-0.427	Te	-0.430	0.022

Table S16: Mulliken charges for pristine $In_{10}S_{12}$ QD (Table A) and Zr-doped In_9S_{12} QD (Table B) with spin densities.

Atom	Pristine (A)		Doped (B)		
	Element	Charge (e)	Element	Charge (e)	Spin Density (μ_B)
1	In	0.816	In	0.804	0.028
2	S	-0.790	S	-0.810	-0.011
3	In	0.816	In	0.804	0.027
4	S	-0.693	S	-0.693	0.011
5	In	0.378	In	0.377	0.003
6	S	-0.693	S	-0.693	0.011
7	S	-0.707	S	-0.673	0.022
8	In	0.816	In	0.804	0.028
9	S	-0.790	S	-0.810	-0.011
10	In	0.616	Zr	0.651	2.728
11	In	0.816	In	0.804	0.028
12	S	-0.693	S	-0.692	0.011
13	In	0.378	In	0.377	0.003
14	S	-0.693	S	-0.692	0.011
15	S	-0.707	S	-0.673	0.022
16	In	0.816	In	0.804	0.028
17	S	-0.790	S	-0.810	-0.011
18	S	-0.707	S	-0.673	0.022
19	In	0.816	In	0.804	0.027
20	S	-0.693	S	-0.693	0.011
21	In	0.378	In	0.377	0.003
22	S	-0.693	S	-0.693	0.011

Table S17: Mulliken charges for pristine $In_{10}Se_{12}$ QD (Table A) and Mo-doped In_9Se_{12} QD (Table B) with spin densities.

Atom	Pristine (A)		Doped (B)		
	Element	Charge (e)	Element	Charge (e)	Spin Density (μ_B)
1	In	0.664	In	0.647	0.023
2	Se	-0.697	Se	-0.661	-0.004
3	In	0.665	In	0.647	0.023
4	Se	-0.620	Se	-0.619	0.019
5	In	0.328	In	0.317	-0.001
6	Se	-0.619	Se	-0.619	0.019
7	Se	-0.579	Se	-0.549	0.004
8	In	0.665	In	0.647	0.023
9	Se	-0.697	Se	-0.661	-0.004
10	In	0.575	Mo	0.511	4.754
11	In	0.665	In	0.647	0.023
12	Se	-0.619	Se	-0.619	0.019
13	In	0.328	In	0.317	-0.001
14	Se	-0.619	Se	-0.619	0.019
15	Se	-0.579	Se	-0.549	0.004
16	In	0.665	In	0.647	0.023
17	Se	-0.697	Se	-0.661	-0.004
18	Se	-0.579	Se	-0.549	0.004
19	In	0.664	In	0.647	0.023
20	Se	-0.619	Se	-0.619	0.019
21	In	0.328	In	0.317	-0.001
22	Se	-0.619	Se	-0.619	0.019

Table S18: Mulliken charges for pristine $In_{10}Te_{12}$ QD (Table A) and Mo-doped In_9Te_{12} QD (Table B) with spin densities.

Atom	Pristine (A)		Doped (B)		
	Element	Charge (e)	Element	Charge (e)	Spin Density (μ_B)
1	In	0.427	In	0.404	0.023
2	Te	-0.542	Te	-0.435	-0.003
3	In	0.426	In	0.405	0.023
4	Te	-0.516	Te	-0.517	0.020
5	In	0.283	In	0.265	-0.002
6	Te	-0.516	Te	-0.517	0.020
7	Te	-0.406	Te	-0.368	0.007
8	In	0.426	In	0.404	0.023
9	Te	-0.542	Te	-0.435	-0.003
10	In	0.536	Mo	0.291	4.738
11	In	0.426	In	0.404	0.023
12	Te	-0.516	Te	-0.517	0.020
13	In	0.282	In	0.265	-0.002
14	Te	-0.516	Te	-0.517	0.020
15	Te	-0.406	Te	-0.367	0.006
16	In	0.426	In	0.404	0.023
17	Te	-0.541	Te	-0.435	-0.003
18	Te	-0.406	Te	-0.367	0.006
19	In	0.426	In	0.404	0.023
20	Te	-0.516	Te	-0.517	0.020
21	In	0.282	In	0.265	-0.002
22	Te	-0.516	Te	-0.517	0.020

Table S19: Mulliken charges for pristine $Tl_{10}S_{12}$ QD (Table A) and Mn-doped Tl_9S_{12} QD (Table B) with spin densities.

Atom	Pristine (A)		Doped (B)		
	Element	Charge (e)	Element	Charge (e)	Spin Density (μ_B)
1	Tl	0.772	Tl	0.737	0.003
2	S	-0.801	S	-0.754	0.043
3	Tl	0.772	Tl	0.766	0.003
4	S	-0.708	S	-0.683	0.016
5	Tl	0.475	Tl	0.464	0.003
6	S	-0.708	S	-0.741	0.025
7	S	-0.688	S	-0.635	0.008
8	Tl	0.772	Tl	0.767	0.002
9	S	-0.801	S	-0.776	0.041
10	Tl	0.661	Mn	0.647	4.750
11	Tl	0.772	Tl	0.771	-0.000229
12	S	-0.708	S	-0.707	0.010
13	Tl	0.475	Tl	0.477	-0.001
14	S	-0.708	S	-0.698	0.014
15	S	-0.688	S	-0.679	0.112
16	Tl	0.772	Tl	0.624	0.166
17	S	-0.801	S	-0.719	0.104
18	S	-0.688	S	-0.632	0.012
19	Tl	0.772	Tl	0.741	0.008
20	S	-0.708	S	-0.698	0.023
21	Tl	0.475	Tl	0.426	0.002
22	S	-0.708	S	-0.696	0.656

Table S20: Mulliken charges for pristine $Tl_{10}Se_{12}$ QD (Table A) and Mn-doped Tl_9Se_{12} QD (Table B) with spin densities.

Atom	Pristine (A)		Doped (B)		
	Element	Charge (e)	Element	Charge (e)	Spin Density (μ_B)
1	Tl	0.652	Tl	0.616	-0.002
2	Se	-0.725	Se	-0.677	0.056
3	Tl	0.652	Tl	0.601	0.113
4	Se	-0.650	Se	-0.677	0.344
5	Tl	0.432	Tl	0.393	0.018
6	Se	-0.650	Se	-0.639	0.018
7	Se	-0.587	Se	-0.593	0.016
8	Tl	0.652	Tl	0.601	0.113
9	Se	-0.725	Se	-0.677	0.056
10	Tl	0.628	Mn	0.559	4.784
11	Tl	0.652	Tl	0.616	-0.002
12	Se	-0.650	Se	-0.639	0.018
13	Tl	0.432	Tl	0.393	0.018
14	Se	-0.650	Se	-0.677	0.344
15	Se	-0.587	Se	-0.514	0.295
16	Tl	0.652	Tl	0.575	0.162
17	Se	-0.725	Se	-0.629	-0.051
18	Se	-0.587	Se	-0.514	0.295
19	Tl	0.652	Tl	0.575	0.162
20	Se	-0.650	Se	-0.583	0.522
21	Tl	0.432	Tl	0.474	0.201
22	Se	-0.650	Se	-0.583	0.522

Table S21: Mulliken charges for pristine $Tl_{10}Te_{12}$ QD (Table A) and Mn-doped Tl_9Te_{12} QD (Table B) with spin densities.

Atom	Pristine (A)		Doped (B)		
	Element	Charge (e)	Element	Charge (e)	Spin Density (μ_B)
1	Tl	0.469	Tl	0.462	0.038
2	Te	-0.614	Te	-0.475	-0.033
3	Tl	0.469	Tl	0.461	0.032
4	Te	-0.575	Te	-0.584	0.117
5	Tl	0.405	Tl	0.382	-0.005
6	Te	-0.575	Te	-0.586	0.130
7	Te	-0.450	Te	-0.417	0.112
8	Tl	0.469	Tl	0.462	0.032
9	Te	-0.614	Te	-0.476	-0.033
10	Tl	0.612	Mn	0.266	4.862
11	Tl	0.469	Tl	0.462	0.037
12	Te	-0.575	Te	-0.586	0.128
13	Tl	0.405	Tl	0.382	-0.005
14	Te	-0.575	Te	-0.584	0.116
15	Te	-0.450	Te	-0.418	0.112
16	Tl	0.469	Tl	0.464	0.028
17	Te	-0.614	Te	-0.481	-0.026
18	Te	-0.450	Te	-0.418	0.111
19	Tl	0.469	Tl	0.464	0.028
20	Te	-0.575	Te	-0.582	0.112
21	Tl	0.405	Tl	0.382	-0.005
22	Te	-0.575	Te	-0.582	0.113

9 Analysis of Vibrational Response

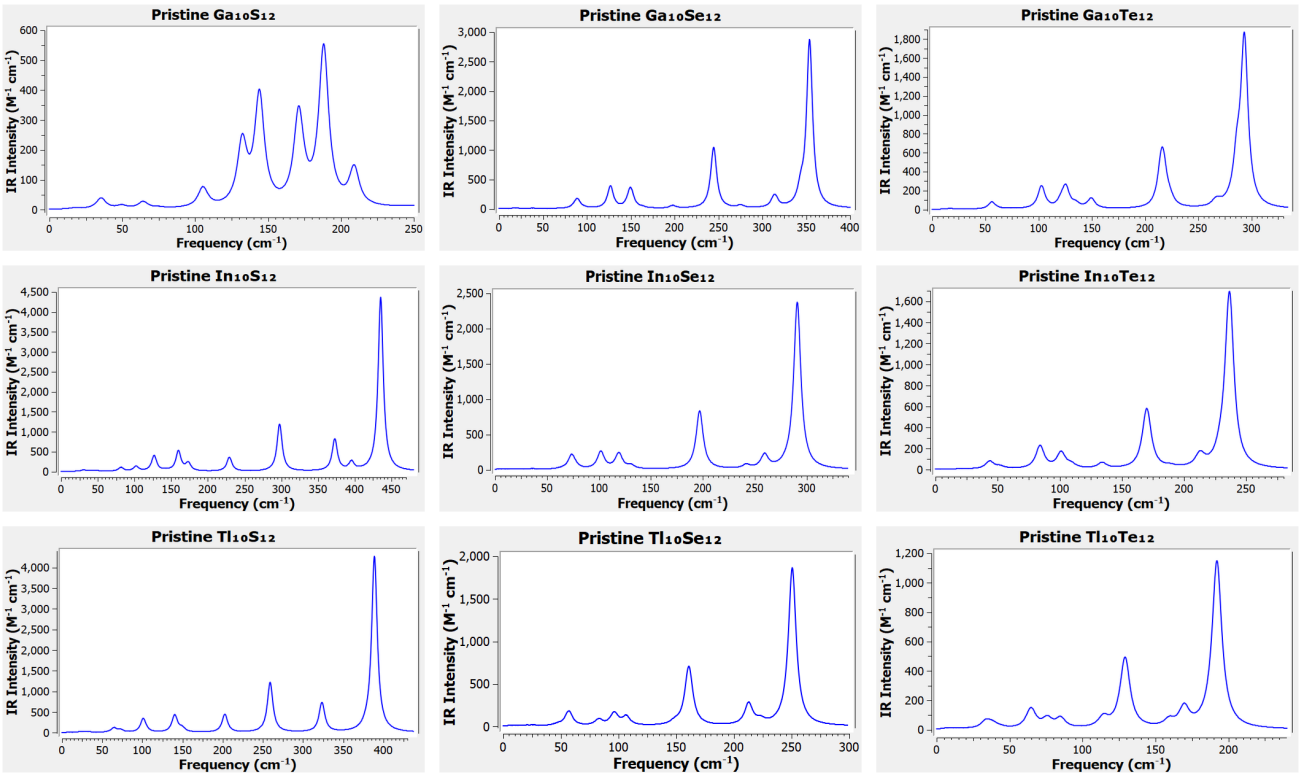

S3(a)

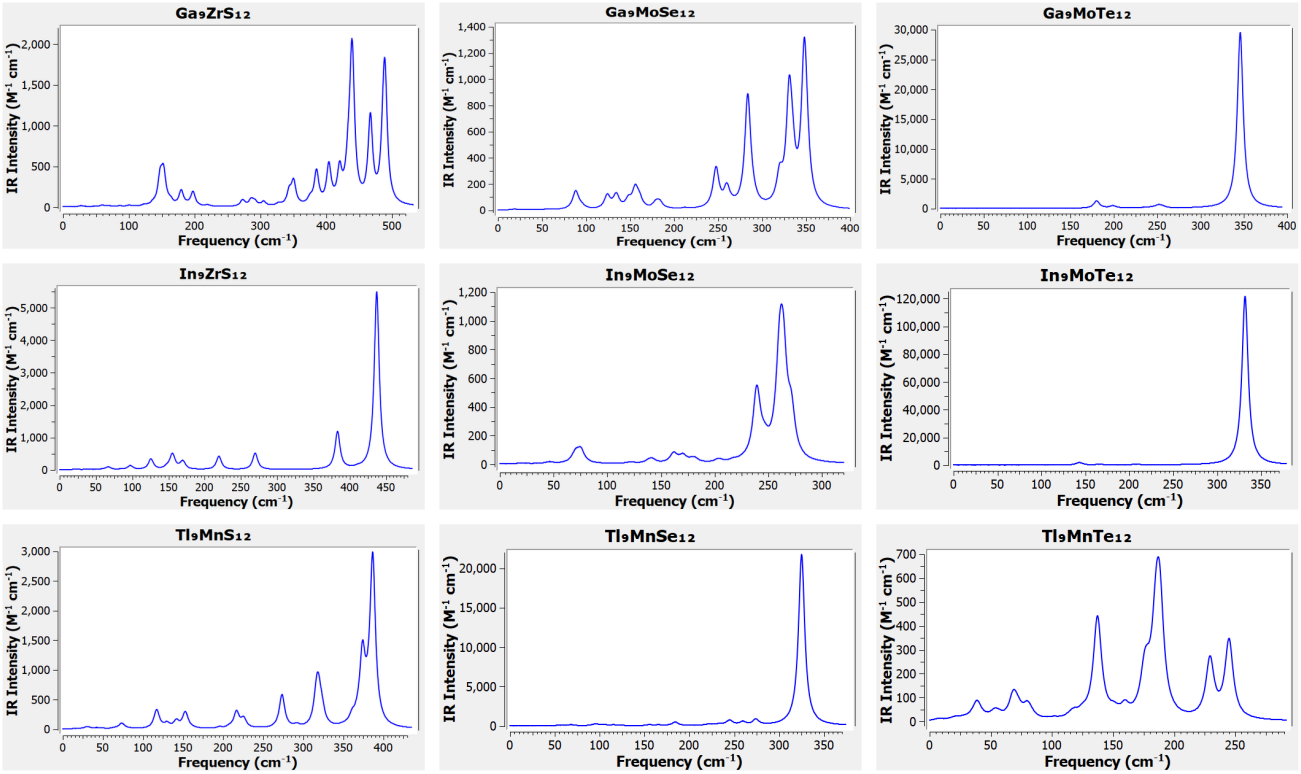

S3(b)

Figure S3(a–b): The IR spectra of the pristine and center-substituted configurations are presented for each of the group. This analysis shows that all the vibrational frequencies are real, with no imaginary vibrations, which ensures the systems occupy stable minima on the potential energy landscape and indicates structural stability.

10 Energy Landscape under Finite-Temperature Perturbations

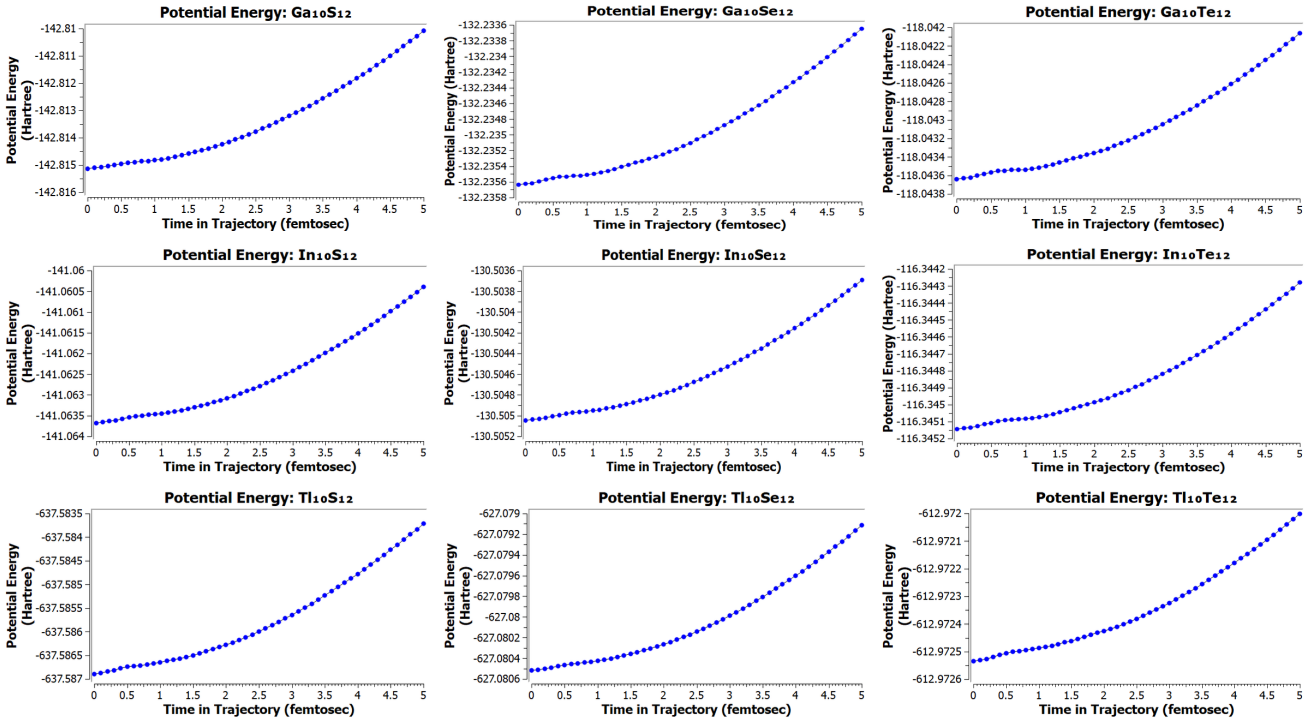

S4(a)

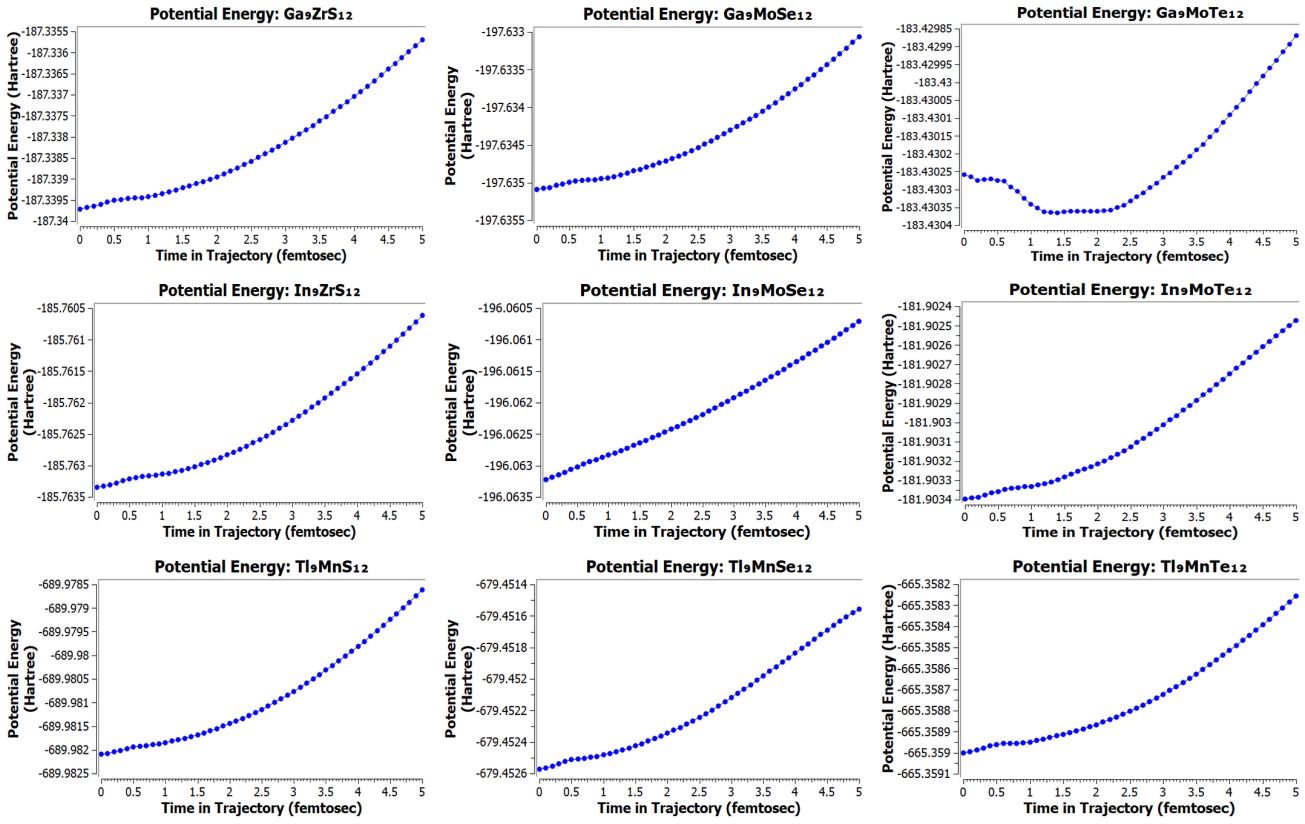
Potential Energy: Ga9ZrS12
Potential Energy: Ga9MoSe12
Potential Energy: Ga9MoTe12
Potential Energy: In9ZrS12
Potential Energy: In9MoSe12
Potential Energy: In9MoTe12
Potential Energy: Tl9MnS12
Potential Energy: Tl9MnSe12
Potential Energy: Tl9MnTe12
Potential Energy (Hartree)
Time in Trajectory (femtosec)

S4(b)

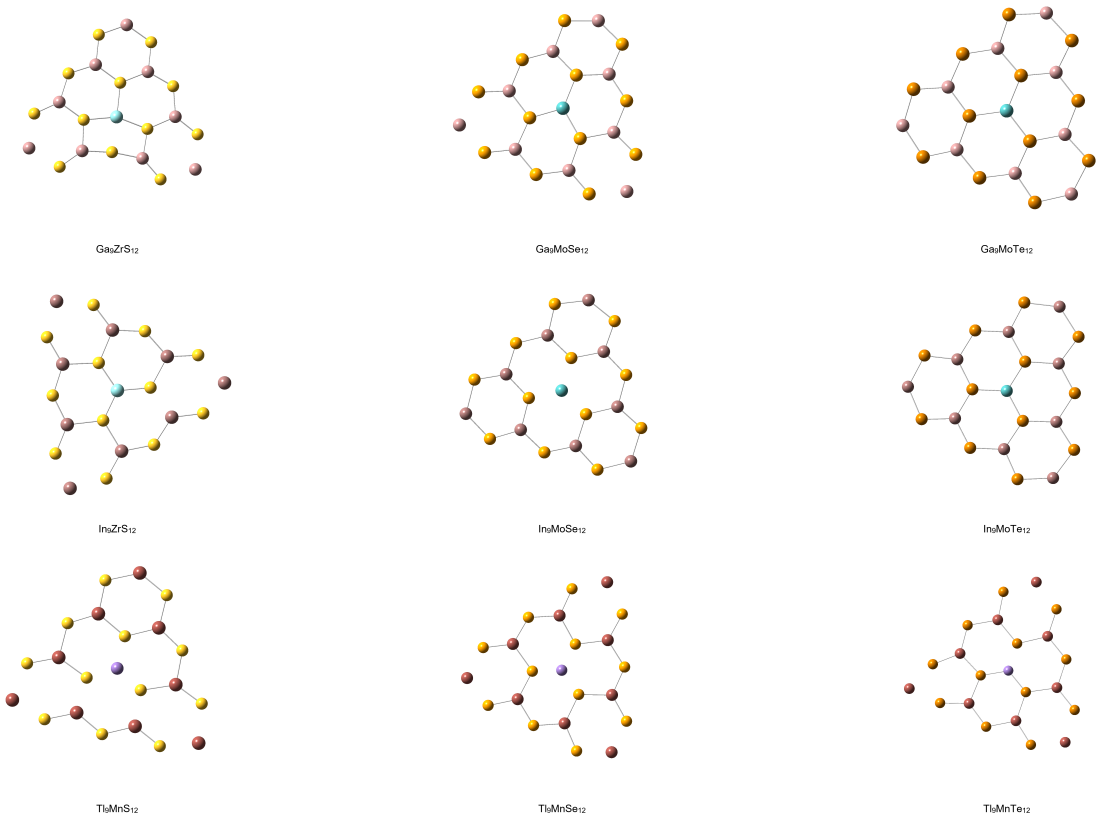

S4(c)

Figure S4(a–c): The ab initio molecular dynamics (AIMD) simulations were performed at an instantaneous temperature of 300 K (room temperature) to study the thermal stability of the configurations, i.e., how the potential energy change over a finite time (5 femtoseconds). As depicted, the changes in potential energies are very small and show smooth variations, with no sudden, large or abrupt fluctuations in energy or geometry. This suggests that the considered systems are thermally stable within the studied temperature range. During the simulation, some bonds present in the initial geometry are no longer observed in the final structure. This is due to thermal fluctuations and structural relaxation, which allow the system to reach a lower-energy configuration. These atoms remain physically interacting, with few covalent bonds are effectively elongated, as also observed from the bond-length vs. time analysis.

11 Structural Data Availability

The optimized molecular structures of all nanodots studied in this work are provided in `.mol` format and deposited on Zenodo at Chowdhury, S. M., & Akther, S. (2025). *Molecular Structure Files for Spin-Selective Orbital Reconfiguration and Colossal Nonlinear Anisotropy in Defect-Engineered Atomically Thin Quantum Dots*. Zenodo. https://doi.org/10.5281/zenodo.16269514

References

[1] Chai, J.-D.; Head-Gordon, M. Long-range corrected hybrid density functionals with damped atom–atom dispersion corrections. *Physical Chemistry Chemical Physics* 2008, 10 (44), 6615. https://doi.org/10.1039/b810189b.

[2] Hay, P. J.; Wadt, W. R. Ab Initio Effective Core Potentials for Molecular Calculations. Potentials for the Transition Metal Atoms Sc to Hg. *J. Chem. Phys.* 1985, *82* (1), 270–283. https://doi.org/10.1063/1.448799.

[3] Gauss, J.; Ruud, K.; Helgaker, T. Perturbation-dependent atomic orbitals for the calculation of spin-rotation constants and rotational g tensors. *The Journal of Chemical Physics* 1996, *105* (7), 2804–2812. https://doi.org/10.1063/1.472143.

[4] Kurtz, H. A.; Stewart, J. J. P.; Dieter, K. M. Calculation of the nonlinear optical properties of molecules. *J. Comput. Chem.* 1990, *11* (1), 82–87. https://doi.org/10.1002/jcc.540110111.